

Fick's law and phase transitions in the Lorentz circuit

*Original*

Fick's law and phase transitions in the Lorentz circuit / Colangeli, Matteo; Rondoni, Lamberto; Kröger, Martin. - In: PHYSICAL REVIEW. E. - ISSN 2470-0045. - ELETTRONICO. - 113:5(2026), pp. 1-12. [10.1103/tdwk-xnn6]

*Availability:*

This version is available at: 11583/3010909 since: 2026-05-16T14:40:14Z

*Publisher:*

APS

*Published*

DOI:10.1103/tdwk-xnn6

*Terms of use:*

This article is made available under terms and conditions as specified in the corresponding bibliographic description in the repository




*Publisher copyright*

APS postprint/Author's Accepted Manuscript e postprint versione editoriale/Version of Record

This article appeared in PHYSICAL REVIEW. E, 2026, 113, 5, and may be found at <http://dx.doi.org/10.1103/tdwk-xnn6>.  
Copyright 2026 American Physical Society

(Article begins on next page)

# Fick’s law and phase transitions in the Lorentz Circuit

Matteo Colangeli <sup>1,\*</sup> Lamberto Rondoni <sup>2,3,†</sup> and Martin Kröger <sup>4,5,‡</sup>

<sup>1</sup>*Department of Information Engineering, Computer Science and Mathematics,  
University of L’Aquila, Via Vetoio, 67100 L’Aquila, Italy*

<sup>2</sup>*Dipartimento di Scienze Matematiche, Politecnico di Torino, Corso Duca degli Abruzzi 24, Turin, Italy*

<sup>3</sup>*INFN, Sezione di Torino, Via P. Giuria 1, 10125 Turin, Italy*

<sup>4</sup>*Magnetism and Interface Physics, Department of Materials,  
ETH Zurich, Hönggerbergring 64, CH-8093 Zurich, Switzerland*

<sup>5</sup>*Computational Polymer Physics, Department of Materials,  
ETH Zurich, Leopold-Ruzicka-Weg 4, CH-8093 Zurich, Switzerland*

Nonequilibrium steady states are investigated in a two-dimensional billiard table, called the Lorentz Circuit, consisting of two circular urns connected by two rectangular strips: an active channel, where a feedback mechanism operates, and a passive finite-size Lorentz channel, which is a finite network of Sinai billiards, *i.e.* a specific environment populated with an array of circular scatterers of fixed radius. We show that, in the finite-horizon regime, a variation of any of the four geometrical parameters of the Lorentz channel can trigger a phase transition in the circuit. Our analytic derivations identify the critical parameters governing these transitions and predict whether they are continuous or discontinuous. We find that both transition orders are realized upon changing just one the geometrical parameters. Our analysis further highlights the validity of Fick’s law in the Lorentz channel, which in our model mirrors the validity of Ohm’s law in electrical circuits. All analytic results are corroborated by an extensive set of numerical simulations of the particle dynamics.

## I. INTRODUCTION

The study of nonequilibrium phase transitions in particle systems coupled to external reservoirs remains a central subject in nonequilibrium statistical mechanics [1–10]. This line of research is motivated by both fundamental considerations and its relevance to driven transport, biological systems, and materials maintained far from equilibrium [11–14]. In contrast to equilibrium systems, where phase transitions are governed by the minimization of a free energy and by detailed balance, nonequilibrium systems may exhibit spontaneous symmetry breaking, long-range correlations, and stationary states carrying nonzero currents. In particular, particle systems driven out of equilibrium by boundary conditions or bulk forces can develop steady-state phase transitions characterized by changes in the global transport properties [15–20]. An analytically tractable example was presented in Refs. [21, 22], where a phase transition occurring in a stochastic cellular automaton gives rise to a stationary particle current consistent with Fick’s law of transport. The model consists of particles on a finite one-dimensional lattice interacting via a long-range Kac potential at low temperature [23]. The interplay between the phase transition and Fick’s law was thus underscored as a theoretical challenge that calls for further exploration. Building on this line of research, a deterministic counterpart to the stochastic cellular automaton was proposed in Ref. [24]. There, the system consists of a two-dimensional (2D) billiard table comprising two circular urns connected by two rectangular channels and subject to periodic boundary conditions. A feedback mechanism, acting within one of the two channels (termed the active channel), prevents parti-

cle clogging by limiting the particle number beyond a given threshold. By varying this threshold, the system undergoes a first-order phase transition from a homogeneous phase, in which particles are evenly distributed between the urns, to an inhomogeneous phase characterized by population asymmetry and sustained by a stationary particle current across the billiard table. In this work we replace the empty rectangular channel (referred to as the passive channel) considered in [24] with the finite-size Lorentz channel of Ref. [25]. This is a finite network of Sinai billiards [26, 27], that is an environment populated by circular scatterers of given radius, investigated in various previous works [28–33].

The aim of the present study is two-fold. First, we investigate whether a phase transition can be induced by varying the size or amount of the scatterers and the width or length of the Lorentz channel. Second, since the inhomogeneous phase supports a stationary particle current circulating through the system, we examine whether the flux in the Lorentz channel obeys Fick’s law. To address these questions, we perform extensive simulations of the particle dynamics. In parallel, we develop a theoretical framework taking into account theories for Lorentz and feedback-controlled channels [24, 25, 34–36] to incorporate the effects of the finite size of the Lorentz channel. We note that, whereas earlier studies examined phase transitions driven by feedback mechanisms in billiard tables with void passive channels that offer no resistance to particle transport [24, 37, 38], the present work focuses explicitly on the role of finite-length Lorentz channels. This model can also be interpreted as an electric circuit in which an electromotive force (e.m.f.) is generated by the previously introduced feedback mechanism, and a current arises in a resistive medium, properly described by Ohm’s law. This was not the case in previous works, in which all particles traveled ballistically in straight channels with no obstacles, which means with infinite diffusion coefficient, or infinite conductivity. Obstacles like those of the Lorentz channel, with finite horizon, give in-

\* [matteo.colangeli1@univaq.it](mailto:matteo.colangeli1@univaq.it)

† [lamberto.rondoni@polito.it](mailto:lamberto.rondoni@polito.it)

‡ [mk@mat.ethz.ch](mailto:mk@mat.ethz.ch)

stead rise, in the infinite channel limit, to a finite diffusion coefficient. That coefficient acquires a logarithmic correction when the horizon is infinite [39], which amounts to an interesting parameter dependence of the transport properties, that is largely understood even in higher dimension [40–44]. The phenomenology turns however quite more complex and highly non-trivial when the channel is finite, as proven in e.g. [28] and more recently in [25]. The behavior under parameters variations of the current driven by the e.m.f. is to be understood, especially in case intends to model small circuits, which is a very active research field, see e.g. Refs.[45–48]. Here, we show that, given a suitable feedback mechanism, a nonequilibrium steady state can be induced within the billiard table by appropriately tuning the density or the size of the circular scatterers. This leads to nonequilibrium phase transitions between different transport regimes. We provide a complete theoretical framework, that captures even quantitatively the dependence of the transport phenomena. The corresponding analytical expressions are further supported by numerical simulations.

The manuscript is structured as follows. Section II introduces the Lorentz Circuit (LC), its eight independent parameters, and the relevant observables. Section III outlines the theoretical framework and characterizes the observed phase transition and the transport properties of the LC. The nature of the phase transition occurring in the LC is worked out, and the derivation of critical system parameters is provided in Section IV. Final remarks and conclusions are drawn in Section V.

## II. THE LORENTZ CIRCUIT

Consider a system of  $N$  point particles moving at constant speed  $v$  within the 2D billiard table  $\Omega \subset \mathbb{R}^2$ , composed of two near-circular urns of equal radius  $r$  connected by two rectangular channels (see Figs. 1 and 2). Particles undergo specular reflections upon colliding with the boundary  $\partial\Omega$ . Following the terminology introduced in [38], we distinguish between an “active channel”, which implements a dynamical rule that mimics an external feedback process [24, 37, 49], and a “passive channel”, where no such mechanism operates. The active channel consists of two identical halves, referred to as gates, shown as the gray shaded regions in Fig. 1. Within each gate, a feedback mechanism operates by *counting* particles: whenever the number of particles entering the gate from the adjacent urn exceeds a fixed threshold, the horizontal component of their velocity is instantaneously reversed, as if they had collided with a vertical wall. This dynamical rule effectively induces a mean-field type interaction among all particles present within each gate and mimics the action of a blind Maxwell’s demon [38]. The demon is termed “blind” because the same rule is applied independently and simultaneously in both gates of the active channel (as indicated by the two particle counters shown above the gates in Fig. 1), thereby introducing no preferential direction for particle transport between the two urns. Phase transitions are nucleated by microscopic, unpredictable, fluctuations [24, 38].

Figure 2 shows the right half ( $x \geq 0$ ) of the billiard system,

showing the right urn (denoted urn 1), with the adjacent gate on the right and half of the passive channel populated with scatterers on the left. Periodic boundary conditions are imposed along the horizontal  $x$ -direction, effectively closing the domain into a circuit containing two urns and two channels. We refer to this setup as the Lorentz Circuit (LC).

The passive channel of the LC is constructed by arranging  $n_x \times n_y$  identical, disjoint elementary cells (each of width  $h$  and length  $\sqrt{3}h$ ) in a grid. The total length and width of the passive channel are  $\ell_p = n_x\sqrt{3}h$  and  $w_p = n_yh$ , respectively. Each cell contains a circular scatterer centered at its midpoint, along with four additional quarter-circle scatterers placed at its corners, as shown in Fig. 3. All scatterers have radius  $s$ , with  $0 \leq s \leq h/2$ , ensuring no overlap. This specific geometric configuration coincides with the finite-size Lorentz channel studied in [25]. In the sequel we describe the geometry of the elementary cell in terms of the dimensionless parameter  $\Phi \in [0, 1]$  and the number density of scatterers  $n \geq 0$ , respectively defined as

$$\Phi = \left(\frac{2s}{h}\right)^2, \quad n = \frac{2}{\sqrt{3}h^2}, \quad (1)$$

where  $\Phi$ , called reduced area fraction, represents the ratio of two quantities: one is the fraction of the area of a cell occupied by the scatterers, and the other is the same fraction evaluated at  $s = h/2$ , i.e. the geometrical scenario in which the circular scatterers touch tangentially one another. Note that  $\Phi = 0$  corresponds to an empty channel, as considered e.g. in [24], whereas the critical value  $\Phi_o$ , marking the transition from the finite to infinite horizon case, is realized for  $\sqrt{3}h = 4s$ , corresponding to  $\Phi_o = 3/4$ . In this work we focus on the finite horizon regime, corresponding to  $\Phi \in [\Phi_o, 1)$ .

The active channel is a rectangular strip of length  $\ell_a$  and width  $w_a$ , subdivided into two empty gates of equal length  $\ell_a/2$ . It is within this region that a feedback mechanism operates via the following dynamical rule: whenever the number of particles in a gate moving toward the opposite gate exceeds a prescribed threshold  $\Theta \in \mathbb{N}$ , the horizontal component of the velocity of all particles present in that gate is instantaneously reversed,  $v_x \rightarrow -v_x$ .

Apart from  $r$  and  $v$ , which we choose to set the unit length and time scale via  $r = v = 1$ , the LC is characterized by eight independent dimensionless parameters:  $n_x$ ,  $n_y$ ,  $\Phi$ ,  $\Theta$ ,  $n$ ,  $w_a$ ,  $\ell_a$ , and  $N$ , which emerge naturally from the freedom to choose units of length and time and because we prefer to have the integer-valued parameters  $n_x$ ,  $n_y$ ,  $\Theta$ , and  $N$  in this list. While  $n_x$ ,  $n_y$ ,  $\Phi$  and  $n$  characterize the passive channel,  $w_a$ ,  $\ell_a$ , and  $\Theta$  define the active channel. For clarity, we are going to mention the dependency on a subset of these 8 parameters, whenever useful. For example, one has  $w_p = w_p(n_y, n)$  and  $\ell_p = \ell_p(n_x, n)$  from Eq. (1). The area of the near-circular urn (Fig. 2) is given by  $A_u(n_y, n, w_a) = \pi + \sum_{c \in \{a, p\}} [w_c x_c / 2 - \sin^{-1}(w_c/2)]$ , where  $x_c^2 = 1 - w_c^2/4$ .

The initial condition for the dynamics is specified by placing all  $N$  particles randomly in one of the two urns, with isotropically distributed velocity directions and fixed speed  $v$ . A relevant observable capturing the dynamic behavior of the

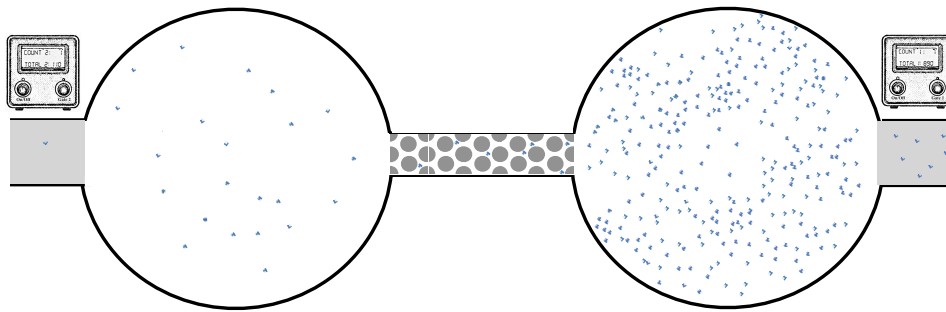


Figure 1. **Lorentz Circuit.** The 2D billiard table  $\Omega \subset \mathbb{R}^2$  consists of two identical near-circular urns interconnected by two rectangular channels. The first is a finite-horizon *passive* Lorentz channel (at the center of the figure), filled with circular scatterers pinned on a triangular lattice. The second channel, called *active*, is divided into two halves, referred to as *gates* (gray shaded regions), where a bounce-back (feedback) mechanism is implemented via a particle (blue dots) counter, depicted above each gate. Periodic boundary conditions are imposed along the horizontal direction, making the billiard table  $\Omega$  a closed circuit.

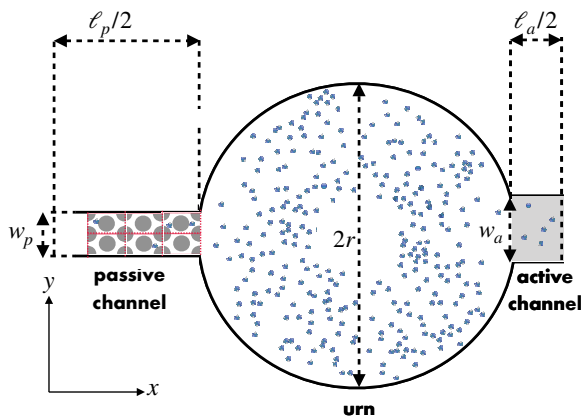


Figure 2. **Magnification** of the right half ( $x \geq 0$ ) of the 2D billiard table  $\Omega$  portrayed in Fig. 1, showing a near-circular urn (urn 1) of radius  $r$  and area  $A_u$ , glued to two rectangular channels: an “active” gate, and half of a finite-horizon “passive” Lorentz channel of length  $\ell_p$  and width  $w_p$ , filled with  $n_x \times n_y$  elementary Lorentz cells (Fig. 3). The full system is made of two such halves, the one shown, and a vertically mirrored one ( $x \leq 0$ , containing urn 2), joined together and subjected to periodic boundary conditions, so that the two active gates constitute an active channel of length  $\ell_a$  and width  $w_a$ .

system is the mass spread

$$\chi(t) = \frac{N_1(t) - N_2(t)}{N}, \quad (2)$$

where  $N_1(t)$  and  $N_2(t)$  denote the transient number of particles residing in urn 1 and urn 2, respectively, at time  $t$ . A second quantity of particular relevance for the present work is the net current. It is defined by taking the difference of number of particles coming from opposite directions and crossing the vertical line separating the two active gates, and by then dividing this quantity by the elapsed time. We denote as  $\bar{\chi} = \lim_{T \rightarrow \infty} T^{-1} \int_0^T \chi(t) dt$  the long time average of the mass spread, provided that the limit exists. Moreover, we also denote and by  $\mathcal{I}$  the stationary net current. The latter is identical with the mean horizontal component  $\langle v_x \rangle$  of the particle velocities, divided by horizontal system size  $L$ , i.e.,

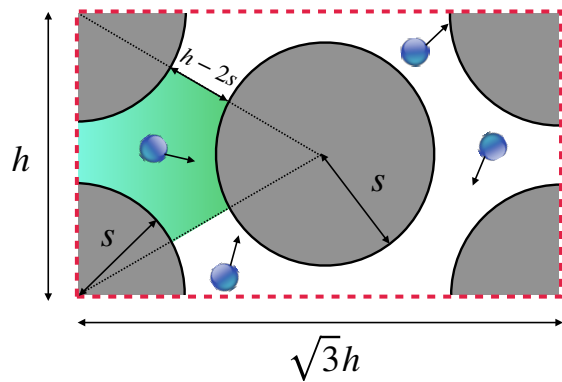


Figure 3. **Elementary cell** of height  $h$ , accessed by a point particle (blue disk) in the passive Lorentz channel (Fig. 2) carrying circular scatterers of radius  $s$ . The green shaded area highlights an individual trapping region discussed in [34], whose three entries/exits all have identical length  $h - 2s$ . In place of  $h$  and  $s$  we use the reduced area fraction of scatterers  $\Phi$  and the circle number density  $n$  (1) to characterize the elementary cell. The gap size in terms of  $\Phi$  and  $n$  is then  $h - 2s = (1 - \sqrt{\Phi})h = 3^{-1/4}(1 - \sqrt{\Phi})\sqrt{2/n}$ .

$\mathcal{I} = -\langle v_x \rangle N/L$  [35], and allows to calculate  $\mathcal{I}$  without inspecting particle positions. The LC is solved numerically using  $N$  point particles (Appendix A) but the calculations can rapidly become highly time-consuming for large  $\Phi$  and large  $n_x$ . An estimate of the computational effort will also be made in Appendix A based on our theoretical relationships.

### III. THEORETICAL APPROACH

In this section, we extend the theoretical framework developed for the 2D model studied in Ref. [24], incorporating the effects of a finite-length Lorentz channel with finite horizon. While the LC is not restricted to the finite horizon regime, theoretical expressions mentioned below, to which we aim to compare, are valid only within this regime [50].

### A. Lorentz channel

We begin by summarizing some important results obtained from previous analytic theoretical work by Zwanzig and the authors on the individual, passive Lorentz channel [25, 34] which constitutes an integral part of our LC. The channel crossing probability of a particle entering the Lorentz channel from an urn with (sinusoidally distributed) velocity at the channel entry which takes the form [25]

$$P(\Phi, n_x) = \frac{p(\Phi)}{p(\Phi) + [4 - 3p(\Phi)]n_x}, \quad (3)$$

where  $p = p(\Phi)$  is a numerically accessible trap crossing probability, again assuming a sinusoidal velocity profile at the trap entry. In [25], this probability was computed numerically as a function of the dimensionless separation parameter  $W = (h - 2s)/s$ , and an analytical approximation thereof, denoted by  $\alpha(W)$ , was also derived. Using  $W(\Phi) = -2 + 2/\sqrt{\Phi}$ , we will denote hereafter  $\tilde{p}(\Phi) = (\alpha \circ W)(\Phi)$ . Strictly,  $P$  does not depend on  $n_y$  for symmetry reasons. One has  $\lim_{\Phi \rightarrow 1} p(\Phi) = 2/3$  and thus  $\lim_{\Phi \rightarrow 1} P(\Phi, n_x) = (1 + 3n_x)^{-1}$ , while  $\lim_{\Phi \rightarrow 0} p(\Phi) = 1$  and  $\lim_{\Phi \rightarrow 0} P(\Phi, n_x) = (1 + n_x)^{-1}$  just formally. As discussed earlier [25], Eq. (3) cannot be applied to  $\Phi < \Phi_o$ , and  $P = 1$  for the empty passive channel, corresponding to  $\Phi = 0$ . The mean time a particle spends in an individual trap is known exactly [34],

$$\tau_{\text{trap}}(\Phi, n) = \frac{\pi(6 - \sqrt{3}\pi\Phi)}{12^{5/4}\sqrt{3n}(1 - \sqrt{\Phi})}. \quad (4)$$

Similarly, from [25], one infers the mean number of collisions inside a trap,

$$c_{\text{trap}}(\Phi) = \frac{\pi\sqrt{\Phi}}{6(1 - \sqrt{\Phi})}, \quad (5)$$

the mean time  $\tau_p^{\rightarrow}$  to cross the passive channel, the mean time  $\tau_p^{\leftarrow}$  to backscatter from the passive channel, and the mean residence time  $\tau_p$  in the passive channel for  $\Phi > \Phi_o$  [25],

$$\begin{aligned} \tau_p(\Phi, n_x) &= P\tau_p^{\rightarrow} + (1 - P)\tau_p^{\leftarrow} \\ &= [4p(\Phi)\tau_{\text{trap}}^{\rightarrow} + [6 - 4p(\Phi)]\tau_{\text{trap}}^{\leftarrow}] n_x. \end{aligned} \quad (6)$$

Using our approximate  $\tau_{\text{trap}}^{\leftarrow} \approx \tau_{\text{trap}}/3[1 - p(\Phi)]$  and  $\tau_{\text{trap}}^{\rightarrow} \approx 2\tau_{\text{trap}}/3p(\Phi)$  [25],

$$\tau_p \approx 6fn_x\tau_{\text{trap}}, \quad f(\Phi) \equiv \frac{7 - 6p(\Phi)}{9[1 - p(\Phi)]}, \quad (7)$$

so that  $\lim_{\Phi \rightarrow 1} \tau_p/n_x = 6\tau_{\text{trap}}$ , where we have introduced a factor  $f$  that is generally close to unity for  $\Phi > \Phi_o$ .

### B. Circuit setup

Next, we follow the guidelines introduced in [24], which refer to billiard tables with void passive channels, and modify the theoretical framework to account for (i) the effective

width  $\tilde{w}_p$  of the Lorentz channel due to its geometry-dictated opening fraction  $(h - 2s)/h$  (Fig. 3), or equivalently,

$$\tilde{w}_p(n_y, \Phi, n) = (1 - \sqrt{\Phi})w_p, \quad (8)$$

and (ii) the above-mentioned crossing probability  $P(\Phi, n_x)$  within the same channel. As long as the velocity distribution within the two urns remains isotropic and the particles are homogeneously distributed, those entering a channel from the adjacent urn have a mean absolute horizontal velocity component  $v_x = \cos \phi$  (recall  $v = 1$ ) at the channel entry that follows from purely geometrical considerations and is given by [35]

$$\langle |v_x| \rangle_e = \frac{\int_{-\pi}^{\pi} \cos^2(\phi) d\phi}{\int_{-\pi}^{\pi} |\cos \phi| d\phi} = \frac{\pi}{4}. \quad (9)$$

This average should not be confused with the mean  $\langle |v_x| \rangle = (2\pi)^{-1} \int_0^{2\pi} |\cos \phi| d\phi = 2/\pi$  for particles residing within urns. The mean residence time  $\tau_a$  within an active gate of length  $\ell_a/2$  is not just  $\ell_a/2$  divided by  $\langle |v_x| \rangle_e$ , but, as shown in [35], involves a rate, here the mean inverse velocity component, and then reads

$$\tau_a = \frac{\ell_a}{2} \langle |v_x^{-1}| \rangle_e = \frac{\ell_a}{2} \frac{\int_{-\pi}^{\pi} d\phi}{\int_{-\pi}^{\pi} |\cos \phi| d\phi} = \frac{\ell_a}{2\langle |v_x| \rangle} = \frac{\pi\ell_a}{4}. \quad (10)$$

Under the same assumptions the probability  $p_a$  that an urn particle enters an active gate within a fixed time interval  $\delta \ll 1$  is given by

$$\frac{p_a(n_y, n, w_a)}{\delta} = \frac{w_a}{2A_u} \langle |v_x| \rangle = \frac{w_a}{\pi A_u}, \quad (11)$$

where the factor 2 stems from the fraction of particles heading to side of the urn that carries the active channel entry, and where  $A_u$  is the above-mentioned area of a single near-circular single urn. Similarly, the probability  $p_p$  that an urn particle enters the passive channel within a fixed time interval  $\delta \ll 1$  is

$$\frac{p_p(n_y, \Phi, n, w_a)}{\delta} = \frac{\tilde{w}_p}{\pi A_u}, \quad (12)$$

involving the effective width  $\tilde{w}_p$  (8) as particles approaching the passive channel and not hitting any of its  $h - 2s$ -sized entries (there are  $n_y$  of them at each channel entry) get reflected into the urn.

We remark that the expression for  $p_p$  given in Eq. (12) follows from the assumption of ergodicity within the urns, which rigorously holds in the limit of vanishing width of the Lorentz channel [51]. Specifically, it corresponds to the ratio between the phase space volume associated with particles of fixed unit speed that enter a channel of width  $\tilde{w}_p$  from an urn of area  $A_u$  during a small time interval  $\delta$ , which is equal to  $2\tilde{w}_p\delta$ , and the phase space volume associated with particles located inside an urn, given by  $2\pi A_u$  [49]. In the stationary state, with the calculated probability  $p_a$  and time  $\tau_a$  at hand, the mean number of particles that enter the  $j$ -th active gate from urn  $j$  in the time interval  $\tau_a$  is then

$$\lambda_j = \frac{p_a}{\delta} \tau_a \bar{N}_j, \quad j \in \{1, 2\}, \quad (13)$$

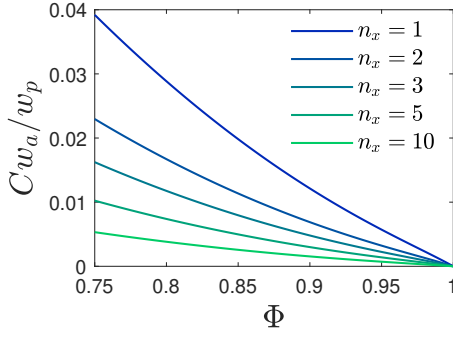


Figure 4. **Theory.**  $Cw_a/w_p$  versus  $\Phi \in [\Phi_o, 1)$  according to Eq. (18) with  $P$  and  $\tilde{w}_p$  from Eqs. (3) and (8).  $C$  monotonically increases with increasing  $W$  and decreasing  $n_x$ . For the Lorentz channel with finite horizon, the upper limit of  $C$  is given by  $C_{\max} \approx 0.04 w_p/w_a$ , in agreement with the figure, using  $p(\Phi_o) \approx 3/4$  from [25].

where  $\bar{N}_j$  is the mean number of particles in urn  $j$ . According to Eq. (13), in the absence of a feedback mechanism, the mean number of particles in the active channel is thus

$$\bar{N}_a = 2(\lambda_1 + \lambda_2), \quad (14)$$

or equivalently

$$\frac{\bar{N}_a}{\bar{N}_1 + \bar{N}_2} = \frac{p_a \pi \ell_a}{\delta} = \frac{w_a \ell_a}{2A_u} = \frac{A_a}{2A_u}, \quad (15)$$

with active area given by  $A_a = w_a \ell_a$ , while the mean number of particles in the passive channel is

$$\begin{aligned} \bar{N}_p &= \frac{p_p}{\delta} (\bar{N}_1 + \bar{N}_2) [P\tau_p^{\leftrightarrow} + (1-P)\tau_p^{\leftarrow}] \\ &= \frac{p_p}{\delta} \tau_p (\bar{N}_1 + \bar{N}_2). \end{aligned} \quad (16)$$

Using Eq. (7) we conclude that the fraction of particles residing in the passive channel,

$$\frac{\bar{N}_p}{\bar{N}_1 + \bar{N}_2} = \frac{f\tilde{A}_p}{2A_u}, \quad (17)$$

is mainly determined by the ratio between the total void area within the passive channel,  $\tilde{A}_p = 2n_x n_y (1 - \phi)/n$ , and the urn areas, as  $f(\Phi)$  defined by Eq. (7) is close to unity and varies over the narrow range  $f \in [0.96, 1.10]$  upon varying  $\Phi \in [\Phi_o, 1)$ . Combining Eqs. (15) and (17) we have quantified the mean stationary fraction of particles residing in channels in terms of LC parameters. In the vicinity of  $\Phi = 1$ , this fraction approaches its largest possible value  $\ell_a w_a / (2\pi + \ell_a w_a)$ , which remains small compared with unity as long as the active channel length  $\ell_a$  does not exceed the urn diameter by far.

### C. Relevant combination of LC parameters

We finally define two parameters  $C$  and  $\lambda$ , that will allow us to calculate  $\bar{\chi}$  and thus the phase boundary of the LC model

using just three parameters, i.e. (i) the threshold  $\Theta$ , (ii) the ratio of probabilities (see Fig. 4),  $C = p_p P / p_a$ , more explicitly,

$$C(\Phi, n, n_x, n_y, w_a) = \frac{\tilde{w}_p(n_y, \Phi, n) P(\Phi, n_x)}{w_a}, \quad (18)$$

and (iii) the estimated mean number of particles entering an active gate in the time interval  $\tau_a/2$ ,

$$\lambda(n, n_y, w_a, \ell_a, N) = \frac{\lambda_1 + \lambda_2}{2} \approx \frac{A_a N}{8A_u}. \quad (19)$$

Here, we made use of Eqs. (10) and (13). Moreover, to simplify the expression, we assumed that the mean number of particles in the urns is much larger than the mean number of particles in the channels. Therefore the two quantities  $C$  and  $\lambda$  are fully determined from  $N$  and the geometrical parameters of the setup  $(n_x, n_y, \Phi, n, w_a, \ell_a)$ , while  $\Theta$  remains an independent parameter of the LC. Note that the stationary  $\bar{\chi}$  can also be expressed in terms of the  $\lambda$ 's,  $\bar{\chi} = (\lambda_2 - \lambda_1)/2\lambda = (\lambda_2 - \lambda)/\lambda$ . Recall that  $C$  and  $\lambda$  are both independent on the form of the stationary velocity distribution, as long as it is well approximated by an even function in  $v_x$ , in other words, as long as there is no significant current  $\mathcal{I}$ . In the absence of the Lorentz scatterers,  $P = 1$  and  $\tilde{w}_p = w_p$ . In that case  $C = w_p/w_a$  recovers its form used in earlier works [24, 35].

### D. Stationary current and mass spread

The stationary net current  $\mathcal{I}_p$  within the passive channel is given by

$$\mathcal{I}_p = \frac{p_p P}{\delta} (\bar{N}_2 - \bar{N}_1), \quad (20)$$

Indeed, Eqs. (3) and (12) show that the quantity  $p_p P / \delta$  represents the probability per unit time that a single particle enters the Lorentz channel and eventually reaches the opposite urn, independently of the distribution of residence times within the urns.

To estimate the stationary net current  $\mathcal{I}_a$  within the active channel, one introduces the probability  $P_{\tau_a, j}$  that at most  $\Theta$  particles enter a gate from the adjacent urn  $j$  in the time interval  $\tau_a$ . Following [24, 49], one finds  $P_{\tau_a, j}(\Theta) = \sum_{n=0}^{\Theta} \lambda_j^n e^{-\lambda_j} / n! = \Gamma(\Theta + 1, \lambda_j) / \Gamma(\Theta + 1)$ , involving Euler's upper incomplete gamma function. The number of particles that cross the  $j$ -th gate is then estimated as the typical number of particles that enter the gate in the time interval  $\tau_a$  conditioned to the fact that such a number is smaller than  $\Theta$  multiplied by  $P_{\tau_a, j}(\Theta) \tau_a / \tau_a$  [24, 49]. The current originating from an urn with  $\bar{N}_j$  particles takes the form  $\tau_a^{-1} \sum_{n=0}^{\Theta} n \lambda_j^n e^{-\lambda_j} / n! = \tau_a^{-1} \lambda_j P_{\tau_a, j}(\Theta - 1)$  for  $j \in \{1, 2\}$ . Hence, the stationary net current in the active channel is finally expressed as  $\mathcal{I}_a = (p_a / \delta) [\bar{N}_1 \Gamma(\Theta, \lambda_1) - \bar{N}_2 \Gamma(\Theta, \lambda_2)] / \Gamma(\Theta)$ . The condition of stationarity requires the equality of the currents  $\mathcal{I}_p$  and  $\mathcal{I}_a$ . Therefore, defining

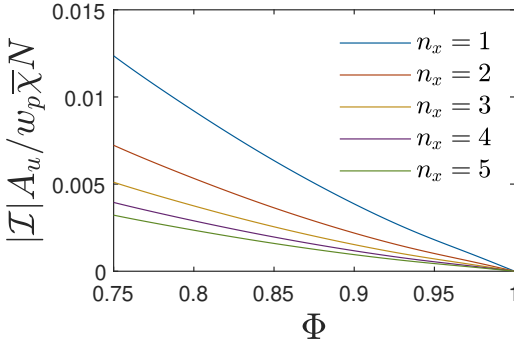


Figure 5. **Theory.**  $|I|A_u/w_p\bar{\chi}N$  according to Eq. (22) and (23) versus  $\Phi \in [\Phi_o, 1)$  for several  $n_x$ .

$\Upsilon \equiv \tau_a(\mathcal{I}_p - \mathcal{I}_a)/2\lambda$ , the condition of stationarity can be written as a nonlinear equation determining  $\bar{\chi}$ ,

$$\Upsilon = \bar{\chi}C + \sum_{\mu \in \{+, -\}} \frac{\mu(1 + \mu\bar{\chi})}{2} \frac{\Gamma[\Theta, (1 + \mu\bar{\chi})\lambda]}{\Gamma(\Theta)} = 0. \quad (21)$$

With a solution  $\bar{\chi}$  at hand, the stationary net current  $\mathcal{I} = \mathcal{I}_a = \mathcal{I}_p$  can be expressed from Eq. (20) as

$$\mathcal{I} = -\frac{p_p P}{\delta} \bar{\chi} N, \quad (22)$$

while (see Fig. 5)

$$\frac{p_p P}{\delta} = \left( \frac{(1 - \sqrt{\Phi})p(\Phi)}{p(\Phi) + [4 - 3p(\Phi)]n_x} \right) \frac{w_p}{\pi A_u}, \quad (23)$$

where the large bracket is the  $\Phi$ - and  $n_x$ -dependent prefactor. For  $p(\Phi) \approx 2/3$ , the large bracket in Eq. (23) simplifies to  $(1 - \sqrt{\Phi})/(1 + 3n_x)$ . To summarize, while  $\bar{\chi}$  is determined via Eq. (21) by  $\Theta$ ,  $C$ , and  $\lambda$ , the current  $\mathcal{I}$  depends on all LC parameters.

### E. Interface equation

In this paragraph we base our arguments on Eq. (21), which can generally be solved only numerically for  $\bar{\chi}$  in terms of  $\lambda$ ,  $\Theta$ , and  $C$ , and derive a so-called interface equation whose solutions determine the phase boundary between homogeneous equilibrium ( $\bar{\chi} = 0$ ) and inhomogeneous nonequilibrium ( $\bar{\chi} > 0$ ) stationary states. We start by noting that one solution to Eq. (21) is  $\bar{\chi} = 0$ , which corresponds to the *equilibrium state*. Furthermore, for certain values of the parameters,  $\Upsilon$  may change sign in intervals not containing  $\lambda$ : such roots, which yield  $\bar{\chi} > 0$ , are nonequilibrium states. Remarkably, Eq. (22) reveals that such LC states are always accompanied by a non-vanishing stationary current  $\mathcal{I}$ , provided that  $C > 0$ . Given its continuity, in those cases in which  $\Upsilon$  vanishes for more than one  $\bar{\chi} \in [0, 1]$ , one may ask which of the steady states of the model is stable. Given the smoothness of  $\Upsilon$ , the linear stability is given by the sign of  $(\partial\Upsilon/\partial\bar{\chi})|_{\bar{\chi}=0}$ .

If the sign is positive the equilibrium state is unstable, if negative it is stable. The points at which the derivative vanishes hence delimit the domain of stability of the equilibrium state. As a definition of such theoretical transition line we consider the locus of points such that  $(\partial\Upsilon/\partial\bar{\chi})|_{\bar{\chi}=0} = 0$ , which thus yields the so-called interface equation

$$\begin{aligned} \mathcal{C}(\Theta, \lambda) &\equiv \frac{\lambda^\Theta e^{-\lambda}}{\Gamma(\Theta)} - \frac{\Gamma(\Theta, \lambda)}{\Gamma(\Theta)} = C, \\ &= \frac{\left(\frac{w_a \ell_a N}{8A_u}\right)^\Theta \exp\left(-\frac{w_a \ell_a N}{8A_u}\right)}{\Gamma(\Theta)} - \frac{\Gamma\left(\Theta, \frac{w_a \ell_a N}{8A_u}\right)}{\Gamma(\Theta)} \\ &= \frac{(1 - \sqrt{\Phi})p(\Phi)n_y h}{w_a p(\Phi) + [4 - 3p(\Phi)]n_x}, \end{aligned} \quad (24)$$

defining  $\mathcal{C}(\Theta, \lambda)$ . In the last two lines of Eq. (24) we made use of the expressions for  $\lambda$  and  $C$  from Eqs. (18) and (19), as well as  $P$  and  $\tilde{w}_p$  from Eqs. (3) and (8) in terms of basic LC parameters to just highlight their role within the interface equation. To be precise, we moreover employed the identities  $w_p = n_y h$  and  $A_a = w_a \ell_a$  in the last step, where we expanded the expression for  $C$ .

This interface equation (24) is fulfilled for any triplets of model parameters  $(\lambda, \Theta, C)$  located at the phase boundary. The interface Eq. (24) cannot be solved analytically for  $\lambda$ , at given  $\Theta$  and  $C$ , but is readily solved numerically. Due to the shape of  $\mathcal{C}$ , for a given pair of model parameters  $(\Theta, C)$ , the system is located in the two-phase region if the positive model parameter  $C$  does not exceed  $C_* = \mathcal{C}(\Theta, \lambda_*)$  with  $\lambda_* = 1 + \Theta$ , because  $\mathcal{C}$  reaches its maximum  $C_*$  at  $\lambda = \lambda_*$ . In that case Eq. (24) has two solutions for  $\lambda$ , bracketing the two-phase region, and the critical point is at  $C = C_*$ . The two-phase region is more or less symmetrically located about the  $\Theta = \lambda - 1$  line. The asymmetry can be traced back to the difference between the principal and non-principal branches of the Lambert function. If  $C$  is fixed, a two-phase region starts to appear as soon as  $\Theta$  exceeds a threshold  $\Theta_*$  that is determined by  $C = \mathcal{C}(\Theta_*, \lambda_*)$ . To summarize, while Eqs. (21) and (22) can be solved for  $\bar{\chi}$  and  $\mathcal{I}$  for given model parameters including the triplet  $(\lambda, \Theta, C)$ , the simpler interface equation suffices to determine the phase boundaries beyond which  $\bar{\chi}$  and  $\mathcal{I}$  both vanish, provided one is interested in exploring the effect of varying one or more of the three parameters.

### F. Fick's Law in the Lorentz channel

To characterize the structure of particle transport in the passive Lorentz channel, let us define the particle flux across the channel,  $\mathcal{J} = \mathcal{I}/w_p$ . For sufficiently large  $n_x$  Eq. (22) with Eq. (23) can be written as in the form of Fick's law [52],

$$\mathcal{J} = -D \mathcal{F}, \quad \mathcal{F} = \frac{\bar{\chi} N}{A_u \ell_p}, \quad (25)$$

with

$$D = \frac{12^{1/4}}{\pi} \frac{(1 - \sqrt{\Phi})p(\Phi)}{4 - 3p(\Phi)} \frac{1}{\sqrt{n}}, \quad (26)$$

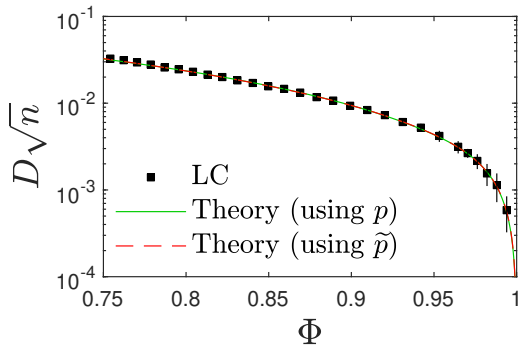


Figure 6. **LC simulations versus theory.** Scaled diffusion coefficient  $D\sqrt{n}$  vs.  $\Phi$ , measured for the LC (filled black squares with error bars) in comparison with the analytical expression (26) evaluated with the numerically calculated  $p(\Phi)$  (dashed green line) and the analytic approximation  $\tilde{p}(\Phi)$  (dashed red line). Remaining LC parameters used in the numerical experiment:  $N = 1000$ ,  $n = 460$ ,  $n_x = \Theta = 5$ ,  $n_y = 1$ ,  $w_a = 0.2$ , and  $\ell_a = 0.3$ .

where we used the identity  $n_x = 12^{-1/4}\sqrt{n}\ell_p$ . Here, we identified  $\mathcal{F}$  with a thermodynamic force corresponding to the finite-difference analogue of the gradient in the stationary particle number density between the urns, and the coefficient  $D$ , expressed by formula (26), with Fick's collective diffusion coefficient in the finite-size Lorentz channel. Figure 6 compares the behavior of the collective diffusion coefficient given by Eq. (26) with the results of numerical simulations of the LC, showing excellent agreement. As  $D$  is monotonically decreasing with increasing  $\Phi$ , and with  $p(\Phi_0) \approx 3/4$ , the upper bound of  $D$  is given by  $D_{\max} \approx 3/[7\pi\sqrt{n}(8 + 14/\sqrt{3})^{1/2}] \approx 0.034/\sqrt{n}$  for the LC with finite horizon. In a typical experiment confirming Fick's law, one has a fixed  $D$  and fixed concentration difference  $\mathcal{F}\ell_p$ , while varying the length of the passive channel. This experiment is reproduced by Fig. 7, which confirms the validity of Fick's law in the Lorentz channel as obtained from the numerical implementation of the Lorentz Circuit, and also demonstrates the excellent agreement between our theoretical predictions (25) and the particle dynamics simulations (Appendix A).

The self-diffusion coefficient  $D_s$  of particles residing within a Lorentz channel had been studied earlier [25, 29, 34, 36]. Using Eq. (26), one obtains  $D = (1 - \pi\Phi/2\sqrt{3})D_s$  for  $n_x \gg 1$ . While the two coefficients are hence identical  $\Phi = 0$ , as expected for a dilute system of non-interacting particles, we find  $D > D_s$ , typical for an attractive system near critical points. In interacting or dense homogeneous systems the ratio  $D_s/D$  is usually identified with the particles' structure factor at zero momentum transfer. Our result thus yields a prediction about the measurable compressibility as a function of  $\Phi$ .

#### IV. PHASE BEHAVIOR

In this section, we investigate in detail the nature of the phase transition emerging within the LC. We begin in

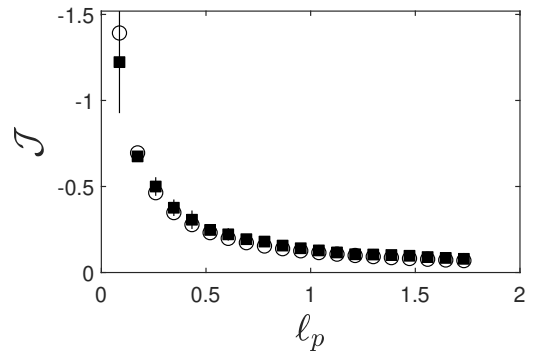


Figure 7. **LC simulations versus theory.** Transport law obtained from LC particle dynamics (filled squares) compared with analytic theoretical prediction without any adjustable parameters (open circles). Shown is the total flux  $\mathcal{J}$  versus  $\ell_p$  at fixed energy difference  $\mathcal{F}\ell_p = 300$  and fixed  $D = 0.008$ . Remaining LC parameters are:  $N = 1000$ ,  $n = 460$ ,  $n_y = 1$ ,  $\Theta = 5$ , and  $w_a = 0.2$ . Essentially varied is only  $n_x$ , while the model parameters  $\ell_a$  and  $\Phi$  are obtained from the two constraints (Fig. 7), as described in Appendix B. Our theoretical derivation predicts the validity of Fick's law and also provides the factor of proportionality (open circles according to Eqs. (25) and (26)), while the simulations of the LC, run for the same set of parameters, are represented by the filled squares. As a by-result the measured  $\mathcal{F}$  coincides within errors with the prescribed value. The agreement is not as convincing if  $w_p$  is not sufficiently small.

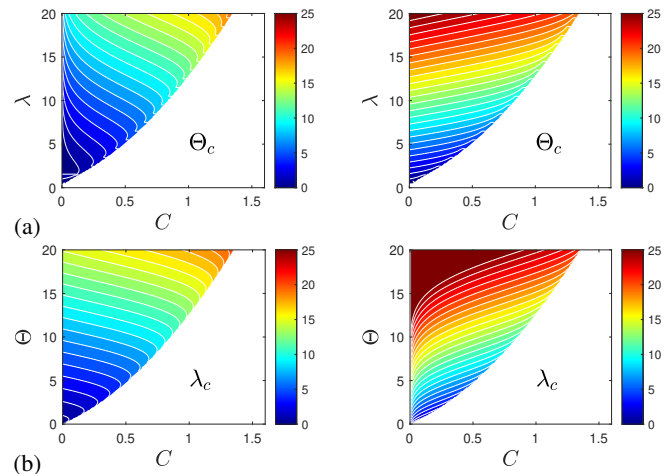


Figure 8. **Implications of the interface equation.** (a) The up to two different critical  $\Theta_c$  (see colorbar) as function of  $C$  and  $\lambda$  obtained by solving the interface equation (24). Contourlines are spaced by unity. Within the white region no solution exists. (b) Similarly, the up to two different critical  $\lambda_c$  (see colorbar) as function of  $C$  and  $\Theta$ .

Sec. IV A by deriving expressions for the critical values of the parameters  $\Phi$ ,  $n$ ,  $n_x$ ,  $n_y$ , which can be tuned to induce a change in the macroscopic phase of the system. Subsequently, in Sec. IV B, we examine the influence of selected parameters in determining whether the resulting phase transition is continuous or discontinuous.

### A. Critical values

The interface equation (24) allows to quantitatively explore the effect of the passive channel geometry ( $\Phi$ ,  $n$ ) and dimensionless size ( $n_x$ ,  $n_y$ ) on the critical values of the LC. To be explicit, we next derive critical values  $\Phi_c$ ,  $n_c$ ,  $n_{x,c}$  and  $n_{y,c}$ . Recall that the effect of the active channel parameters  $\ell_p$ ,  $w_p$ , and  $\Theta$  on the phase diagram in the presence of an empty passive channel ( $\Phi = 0$ ) had been studied earlier. While the independent variation of  $\Theta$  or  $\lambda$  at constant  $C$  gives rise to a re-entrant phenomenon (Fig. 8), realized e.g. upon varying the length  $\ell_a$  of the active channel as it does not affect  $C$ , the situation is very different for the passive channel. Here,  $\lambda$  cannot be varied independently from  $C$  (Fig. 4). As a result, there is a single transition point in both  $\mathcal{F}$  and  $\mathcal{J}$  if one varies just one of the four passive channel parameters, while keeping all other LC parameters unchanged, as demonstrated by Fig. 9. The dashed lines in this figure mark our theoretical predictions derived next.

For the calculation of the critical reduced area fraction  $\Phi_c \in [\Phi_o, 1)$  one has to take into account that  $C$  is affected by  $\Phi$ , while the remaining two variables determining the phase boundary,  $\lambda$  and  $\Theta$ , are unaffected. This implies that  $\Phi_c$  is the solution of the following nonlinear equation,

$$\frac{w_a \mathcal{C}(\Theta, \lambda)}{w_p} = \frac{(1 - \sqrt{\Phi_c})p(\Phi_c)}{p(\Phi_c) + [4 - 3p(\Phi_c)]n_x} \quad (27)$$

with  $\mathcal{C}$  defined in Eq. (24). Equation (27) can be solved numerically, using  $p(\Phi)$  or analytically using  $\tilde{p}(\Phi)$ . The important observation is that the right hand side is monotonically decreasing with increasing  $\Phi_c$ . Its upper bound  $\approx 0.4/(3 + 7n_x) \equiv \varepsilon(n_x) \ll 1$  is therefore estimated from  $0.738 \approx p(\Phi_o) \approx \tilde{p}(\Phi_o) \approx 3/4$ . As long as the left hand side resides beyond this bound, there is no  $\Phi_c$ . Let us therefore consider the case  $w_a \mathcal{C}(\Theta, \lambda)/w_p < \varepsilon(n_x)$ , where exactly one solution  $\Phi_c \in [\Phi_o, 1)$  to Eq. (27) is now known to exist. A simple expression for  $\Phi_c$  is readily available if we let the value of  $p(\Phi)$  at  $\Phi = \Phi_c$  be approximately given by  $p(\Phi_c) \approx 2/3$ , and use  $\varepsilon(n_x) \ll 1$ . This leads to a linear relationship between  $\Phi_c$  and  $n_x$ ,

$$\Phi_c \approx 1 - \frac{2(1 + 3n_x)w_a \mathcal{C}(\Theta, \lambda)}{w_p} \quad (28)$$

for  $w_a \mathcal{C}/w_p < \varepsilon(n_x)$ , excellently confirmed by Fig. 9-a. In light of Eq. (24), where  $\mathcal{C}$  is seen to be of order unity or smaller for  $\lambda, \Theta \leq 20$ , the existence of  $\Phi_c \in [\Phi_o, 1)$  requires an active channel width  $w_a \lesssim w_p/[8(1 + 3n_x)]$  that is not only smaller than  $w_p \ll 1$ , but further decreases with increasing  $n_x$ .

For the calculation of  $n_c$  one has to take into account that both  $C$  and  $\lambda$  are affected by  $n$  via  $w_p \propto n^{-1/2}$ , while the remaining variable determining the phase boundary,  $\Theta$ , is unaffected by  $n$ . The effect of  $n$  on  $\lambda$  is however very weak, corresponding to  $A_u \approx \pi$ . This yields the following explicit expression for the critical number density of scatterers,

$$n_c \approx \frac{2[n_y(1 - \sqrt{\Phi})]^2}{\sqrt{3}[(1 + 3n_x)w_a \mathcal{C}(\Theta, \frac{w_a \ell_a N}{8\pi})]^2}. \quad (29)$$

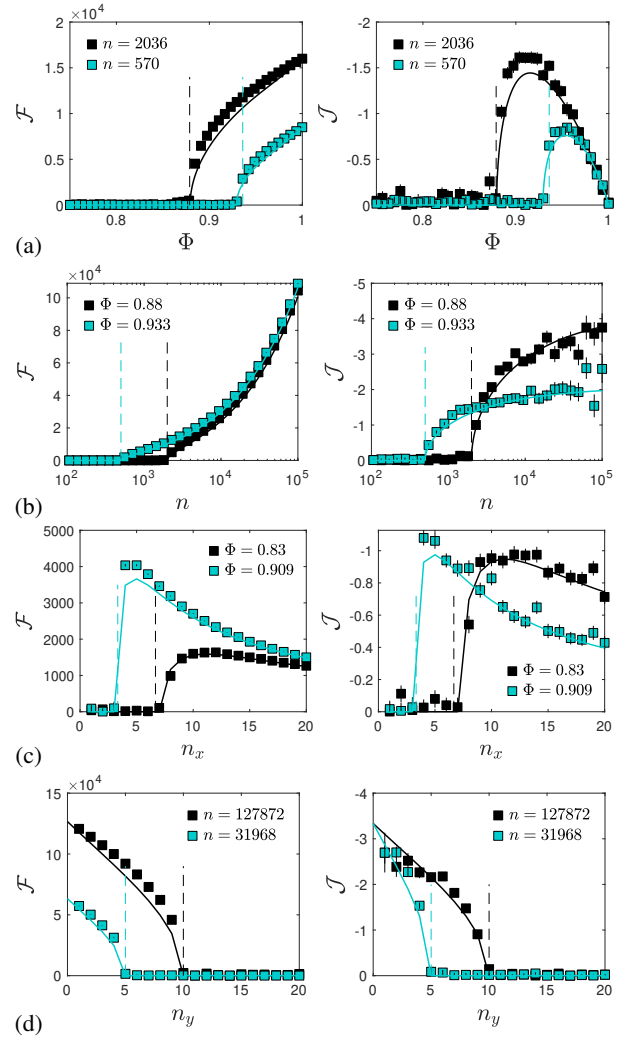


Figure 9. **LC phase transitions.** Thermodynamic force  $\mathcal{F}$  (left column) and corresponding flux  $\mathcal{J}$  (right column) versus (a) area fraction  $\Phi$ , (b) number density of scatterers  $n$ , (c) horizontal number of repeated elementary cells  $n_x$ , and (d) vertical number of repeated elementary cells  $n_y$  at otherwise unchanged LC parameters. The default values are  $N = 10000$ ,  $\Phi = 0.9$ ,  $n = 1000$ ,  $n_x = 3$ ,  $n_y = 1$ ,  $w_a = 0.001$ ,  $\ell_a = 10$ , and  $\Theta = 5$  for all panels. Symbols: results from the LC, with error bars (500 independent realizations for each data point). Solid lines: Eq. (25) evaluated with the numerical solution to Eq. (21). Dashed vertical lines mark our theoretical predictions (28)–(30) for the critical values.

The critical dimensionless sizes  $n_{x,c}, n_{y,c} \in \mathbb{R}^+$  can be estimated along the same lines. Exploiting, as previously done in Sec. III D, the approximation  $p(\Phi) \approx 2/3$ , the resulting analytical expressions take the form:

$$n_{x,c} \approx \frac{1}{3} \left[ \frac{(1 - \sqrt{\Phi})w_p}{w_a \mathcal{C}(\Theta, \lambda)} - 1 \right], \quad (30)$$

$$n_{y,c} \approx \frac{3^{1/4} w_a (1 + 3n_x) \sqrt{n} \mathcal{C}(\Theta, w_a \ell_a N / 8\pi)}{\sqrt{2}(1 - \sqrt{\Phi})},$$

where  $\lambda$  and  $w_p$  were specified earlier in terms of the LC pa-

rameters  $n$ ,  $n_y$ ,  $w_a$ ,  $\ell_a$ , and  $N$ .

Our theoretical predictions for the quantities  $\mathcal{F}$  and  $\mathcal{J}$  exhibit a striking agreement with the numerical solution of Eq. (21). Indeed our numerical simulations, portrayed in Fig. 9, match the theoretical predictions coming from Eqs. (21) and Eq. (30), and reveal that when  $n_x$  grows beyond the critical value  $n_{x,c}$  the LC model switches from a homogeneous to an inhomogeneous state (Fig. 9-c). A similar transition is observed when  $n_y$  is instead decreased below the critical value  $n_{y,c}$  (Fig. 9-d). The nature of all the transitions is explored next.

### B. Continuous versus discontinuous phase transitions

All rows of Fig. 9 evidence the onset of a phase transition, when the four geometrical parameters of the Lorentz channel are varied. In particular, the phase transition appears to be continuous when varying the parameter  $\Phi$  (Fig. 9-a). All critical values are affected by the entire set of the parameters of the LC. Specifically, any of them can be tuned to produce a (continuous) phase transition, provided all others fall within a suitable range. Our analytic expressions provide such ranges, and all critical values (28)–(30) are confirmed by Fig. 9.

To make an example without referring to numerics, if  $\bar{\chi}$  is close to unity beyond a certain  $\Phi_c$ , and close to zero for the empty passive channel, while system parameters  $n_x$ ,  $n_y$ ,  $n$ ,  $N$ ,  $w_a$  (and thus  $A_u$ ) are held constant, as in Fig. 9-a, then  $w_p$  and  $\ell_p$  are constants, and the flux  $\mathcal{J}$  we expect to behave as  $\mathcal{J} \simeq DN/\ell_p A_u$ . Using  $\tilde{p}(\Phi)$  instead of  $p(\Phi)$  in the definition of  $D$  (26), Taylor expansion about  $\Phi = 1$  yields

$$D = \frac{(1 - \Phi)}{3^{3/4} \pi \sqrt{2n}} + \mathcal{O}(1 - \Phi)^2, \quad (31)$$

i.e., one expects  $\mathcal{J}$  to increase linearly with  $\Phi$  for  $\Phi \lesssim 1$ . This implication is in agreement with the numerical result shown in Fig. 9-a (for this panel,  $-\mathcal{J} \simeq 2(1 - \Phi)$ , confirmed by the data).

Next we prove that the LC exhibits both 1st and 2nd order phase transitions depending on the choice of LC parameters. A phase transition shown in Figs. 9-a,b is “continuous” when varying either the parameter  $\Phi$  or  $n$  if the respective condition holds:

$$\lim_{\Phi \rightarrow \Phi_c^+} \mathcal{F} = 0, \quad \lim_{n \rightarrow n_c^+} \mathcal{F} = 0. \quad (32)$$

To investigate the order of the transition, we here follow classical recipes [53]. Taylor-expanding Eq. (21) about  $\mathcal{F} = 0$  yields

$$\Upsilon = a_1 \bar{\chi} - a_3 \lambda^\Theta \bar{\chi}^3 + \mathcal{O}(\bar{\chi}^5) = 0, \quad (33)$$

with coefficients

$$a_1 = C - \mathcal{C}(\Theta, \lambda),$$

$$a_3 = \frac{{}_1F_1(\Theta, \Theta - 1, -\lambda)}{2\Gamma(\Theta - 1)} + \frac{{}_1F_1(\Theta, \Theta - 2, -\lambda)}{6\Gamma(\Theta - 2)}, \quad (34)$$

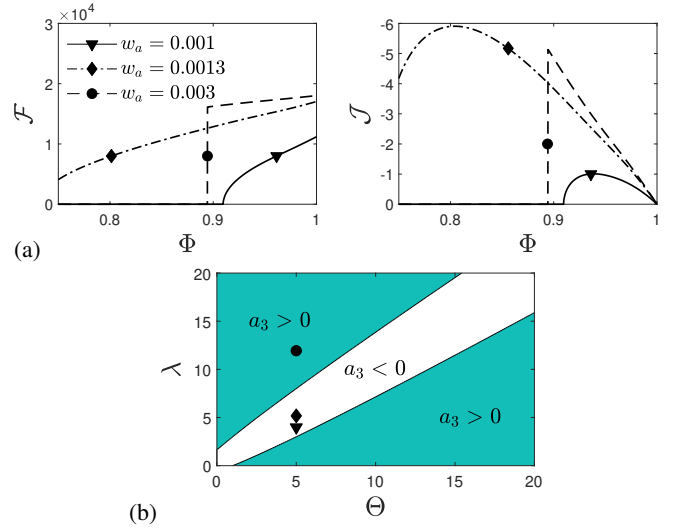


Figure 10. (a) The three possible scenarios upon variation of a single Lorentz channel parameter for  $\mathcal{F}$  and  $\mathcal{J}$ . Here  $\Phi$  is varied over the interval  $[\Phi_o, 1]$  at three different values of the width  $w_a$  of the active channel: (i) Continuous phase transition (solid line), (ii) no phase transition (dot-dashed line), and (iii) discontinuous phase transition (dashed line). Remaining parameters are the ones used for the black squares in Fig. 9-a. (b) Sign of  $a_3$  (34) versus  $\Theta$  and  $\lambda$ . The locations of the three cases are marked by the symbols already used in (a).

involving the hypergeometric  ${}_1F_1$  and gamma function  $\Gamma$  [54], as well as  $C$  and  $\mathcal{C}$  from Eqs. (18) and (24). Note that  $a_3$  – the change of  $\Upsilon$  curvature – does not depend on  $C$ , and that  $a_1$  changes sign at the critical  $C_c = \mathcal{C}$ . Equation (33) without the  $\mathcal{O}(\bar{\chi}^5)$  term is solved by  $\bar{\chi} = 0$  and  $\bar{\chi}^2 = (C - \mathcal{C})/\lambda^\Theta a_3$ . If  $a_3 < 0$  then  $\bar{\chi}$  grows continuously from zero as  $C \rightarrow C_c^-$ : the classic pitchfork bifurcation — a hallmark of a continuous (2nd order) transition. If  $a_3 > 0$ , on the other hand, the LC exhibits a 1st order transition as long as a variable is varied over its critical value calculated in Section IV A. Note that  $a_3$  given by Eq. (34) can have either sign depending on  $\Theta \in \mathbb{N}^+$  and  $\lambda \in \mathbb{R}^+$ , due to the well documented features of  ${}_1F_1$  [54]. While  $a_3 < 0$  within a region next to  $\lambda = \Theta$ ,  $a_3 < 0$  otherwise (Fig. 10-b). The calculations are confirmed by Fig. 10-a. While  $\lambda$  and  $\Theta$  differ by only 20% for  $w_a = 0.001$ , they differ by 139% for  $w_a = 0.003$ . The story is slightly different but similar for  $n$  (here both  $C$ ,  $\lambda$ , and  $\ell_p$  appearing in  $\mathcal{F}$  depend on  $n$ ). Again, depending on the LC parameters, there are both 1st and 2nd order regimes.

## V. CONCLUSIONS

The derivation of Fick’s law in particle systems undergoing a phase transition was presented in Ref. [21], based on the analysis of a stochastic cellular automaton. In the present work, we pursue a related line of investigation by studying the stationary behavior of a deterministic particle model. Building on the geometrical setup of Ref. [24], we introduce an array of circular scatterers into the so-called passive channel, thereby converting it into a finite-size 2D Lorentz chan-

nel [25]. While the current manuscript builds upon previous theoretical results, the characterization of both the Fick's law and the phase transition within the LC model prompted new analytical derivations and a significantly refined numerical implementation of the billiard dynamics.

Our theoretical framework, supported by extensive numerical simulations, predicts the existence of critical values for the scatterer number density, reduced area fraction, and the length and width of the Lorentz channel in the finite-horizon regime, under well-defined conditions. Specifically, the interface equation admits solutions only in certain regions of the parameter space. The critical parameters mark the transition between two distinct phases: a homogeneous phase and an inhomogeneous one. The latter is characterized by a stationary particle current flowing through the Lorentz Circuit. Remarkably, our theory correctly predicts that the phase transition can be either continuous or discontinuous, depending on the values of the model parameters. Furthermore, we verify the validity of Fick's law in the Lorentz channel, which manifests itself as a linear relation between the stationary particle flux and the thermodynamic force associated with the gradient of the stationary particle density across the two urns. In particular, we find excellent agreement between our theoretical predictions and numerical simulations of the particle dynamics, both for the particle current and for the diffusion coefficient, as functions of the geometric parameters of the Lorentz channel, see Figs. 6 and 7. It is also worth underlining that, once a nonequilibrium steady state is established in the Lorentz Circuit, the particle current obeys Fick's (or equivalently in our models, Ohm's) law within the finite-length Lorentz channel, while it flows from the less populated to the more populated urn through the active channel. These findings improve our understanding of the interplay between diffusive transport and phase transitions in a particle model that remains analytically tractable, although with a complex dependence on parameters. In particular, the Lorentz Circuit introduced here extends, within a fully deterministic framework, the phenomenology previously observed in the stochastic circuit model of [55], where particles interacting via a Kac potential give rise to nonequilibrium steady states and uphill currents, see also [21, 23].

Remarkably, we derive an analytical expression for the collective diffusion coefficient linking the thermodynamic force to its conjugate flux. This coefficient depends explicitly on the geometry of the elementary cells within the Lorentz channel. Numerical simulations are found to be in excellent agreement with the theoretical predictions. Additionally, we establish a relation between the self-diffusion coefficient – studied earlier in [25, 34, 36] – and the collective diffusion coefficient evaluated for the LC.

As a future development, we plan to extend this theoretical framework to the Lorentz Circuit with infinite horizon [56–66], as well as to its three-dimensional counterpart. These extensions are expected to reveal new transport regimes and dynamical behaviors. Another important theoretical question, motivated by the periodic arrangement of scatterers in the LC, concerns the possible emergence of particle transport governed by the Fokker–Planck law rather than by Fickian diffusion, as discussed e.g. in Ref. [67].

#### Data availability statement

The data that support the findings of this article are openly available [68].

#### Acknowledgements

The authors thank Emilio N. M. Cirillo (Sapienza University of Rome, Italy) and Sergio Ciliberto (Laboratoire de Physique Ecole Normale Supérieure de Lyon, France) for useful discussions. This work was carried out under the auspices of the Italian National Group of Mathematical Physics. LR gratefully acknowledges support from the Italian Ministry of University and Research (MUR) through the grant PRIN2022-PNRR project (No. P2022Z7ZAJ) “A Unitary Mathematical Framework for Modelling Muscular Dystrophies” (CUP: E53D23018070001). The research of MC has been developed in the framework of the research project National Centre for HPC, Big Data and Quantum Computing - PNRR Project, funded by the European Union - Next Generation EU (CUP: E13C22001000006).

- 
- [1] N. Ruiz-Pino, D. Villarrubia-Moreno, A. Prados, and F. J. Cao-Garcia, Information in feedback ratchets, *Phys. Rev. E* **108**, 034112 (2023).
  - [2] F. Casini, C. Giardina, and C. Vernia, Uphill in reaction-diffusion multi-species interacting particles systems, *J. Stat. Phys.* **190**, 132 (2023).
  - [3] S. Acharya and B. Bagchi, Diffusion in a two-dimensional energy landscape in the presence of dynamical correlations and validity of random walk model, *Phys. Rev. E* **107**, 024127 (2023).
  - [4] F. Nakai, Y. Masubuchi, Y. Doi, T. Ishida, and T. Uneyama, Fluctuating diffusivity emerges even in binary gas mixtures, *Phys. Rev. E* **107**, 014605 (2023).
  - [5] D. Bhattacharyya and C. Jarzynski, From a feedback-controlled demon to an information ratchet in a double quantum dot, *Phys. Rev. E* **106**, 064101 (2022).
  - [6] A. Kononovicius and J. Ruseckas, Stochastic dynamics of n correlated binary variables and non-extensive statistical mechanics, *Phys. Lett. A* **380**, 1582 (2016).
  - [7] A. G. Godizov, Nature of phase transitions (role of the self-consistent feedback in the evolution of material structures), *Russ. Phys. J.* **65**, 63 (2022).
  - [8] A. G. Godizov and A. A. Godizov, On the objective origin of the phase transitions and metastability in many-particle systems, *Int. J. Mod. Phys. B* **28**, 1450163 (2014).

- [9] H. Jiang and Z. Hou, Nonequilibrium dynamics of chemically active particles, *Chin. J. Chem.* **40**, 419 (2022).
- [10] B. Leimkuhler and X. Shang, On the numerical treatment of dissipative particle dynamics and related systems, *J. Comput. Phys.* **280**, 72 (2015).
- [11] J. Marro and R. Dickman, *Nonequilibrium Phase Transitions in Lattice Models* (Cambridge University Press, Cambridge, U.K., 1999).
- [12] B. Schmittmann and R. K. P. Zia, *Statistical Mechanics of Driven Diffusive Systems*, edited by C. Domb and J. L. Lebowitz, Phase Transitions and Critical Phenomena, Vol. 17 (Academic Press, New York, United States, 1995).
- [13] G. Ódor, Universality classes in nonequilibrium lattice systems, *Rev. Mod. Phys.* **76**, 663 (2004).
- [14] H. Hinrichsen, Non-equilibrium critical phenomena and phase transitions into absorbing states, *Adv. Phys.* **49**, 815 (2000).
- [15] H. Spohn, *Large Scale Dynamics of Interacting Particles* (Springer, Berlin, Germany, 1991).
- [16] M. R. Evans and T. Hanney, Nonequilibrium statistical mechanics of the zero-range process and related models, *Journal of Physics A: Mathematical and General* **38**, R195 (2005).
- [17] V. Venkataraman and R. Neelakantan, Nonequilibrium phase transitions – a review, in *Stochastic Processes: Formalism and Applications*, Lecture Notes in Physics, Vol. 638, edited by A. Lakshminarayan and M. Murthy (Springer, Berlin, 2005) pp. 228–237.
- [18] U. C. Täuber, Driven diffusive systems and growing interfaces, in *Critical Dynamics: A Field Theory Approach to Equilibrium and Non-Equilibrium Scaling Behavior* (Cambridge University Press, 2014).
- [19] C. Reichhardt and C. J. Olson Reichhardt, Depinning and nonequilibrium dynamic phases of particle assemblies driven over random and ordered substrates: a review, *Reports on Progress in Physics* **80**, 026501 (2017).
- [20] Y. Baek, Y. Kafri, V. Lecomte, and A. L. Lloyd, Dynamical symmetry breaking and phase transitions in driven diffusive systems, *Physical Review Letters* **118**, 10.1103/PhysRevLett.118.030604 (2017).
- [21] M. Colangeli, A. D. Masi, and E. Presutti, Latent heat and the Fourier law, *Phys. Lett. A* **380**, 1710 (2016).
- [22] M. Colangeli, A. D. Masi, and E. Presutti, Microscopic models for uphill diffusion, *J. Phys. A* **50**, 435002 (2017).
- [23] M. Colangeli, C. Giberti, and C. Vernia, Uphill diffusions in single and multi-species systems, *J. Phys. A* **56**, 393001 (2023).
- [24] E. N. M. Cirillo, M. Colangeli, O. Richardson, and L. Rondoni, Deterministic model of battery, uphill currents, and nonequilibrium phase transitions, *Phys. Rev. E* **103**, 032119 (2021).
- [25] E. N. M. Cirillo, M. Colangeli, M. Kröger, and L. Rondoni, Particle transport and finite-size effects in Lorentz channels with finite horizons, *Physica D* **472**, 134512 (2025).
- [26] M. Budantsev, Z. Kvon, A. Pogosov, G. M. Gusev, J. Portal, D. Maude, N. Moshegov, and A. Toropov, 2D lattice of coupled Sinai billiards: metal or insulator at  $g \ll 1$ ?, *Physica B* **256**, 595 (1998).
- [27] M. V. Budantsev, Z. D. Kvon, A. G. Pogosov, and J. Portal, Order, disorder and chaos in 2D lattice of coupled Sinai billiards, *Phys.-Usp.* **44**, 20 (2001).
- [28] H. Larralde, F. Leyvraz, G. Martinez-Mekler, R. Rechtman, and S. Ruffo, Transmission and scattering of a Lorentz gas on a slab, *Phys. Rev. E* **58**, 4254 (1998).
- [29] E. Toivonen, J. Kaipainen, M. Molkari, J. Keski-Rahkonen, R. Klages, and E. Raesaenen, Anomalous diffusion in the square soft Lorentz gas, *Phys. Rev. E* **111**, 014216 (2025).
- [30] M. J. Lazarotto, I. L. Caldas, and Y. Elskens, Diffusion transitions in a 2D periodic lattice, *Commun. Nonlin. Sci. Numer. Simul.* **112**, 106525 (2022).
- [31] H. Chen, Y. Yang, Z. Yu, M. Zhong, and L. Zhang, Thermal hall effect from a modified Lorentz gas model, *Phys. Rev. E* **101**, 042129 (2020).
- [32] A. K. Karlis, F. K. Diakonou, C. Petri, and P. Schmelcher, Criticality and strong intermittency in the Lorentz channel, *Phys. Rev. Lett.* **109**, 110601 (2012).
- [33] F. Barra, T. Gilbert, and S. Reyes, Conductivity of the self-similar Lorentz channel, *Int. J. Bifurcation Chaos* **19**, 2687 (2009).
- [34] J. Machta and R. Zwanzig, Diffusion in a periodic Lorentz gas, *Phys. Rev. Lett.* **50**, 1959 (1983).
- [35] E. N. Cirillo, M. Colangeli, A. Di Francesco, M. Kröger, and L. Rondoni, Particle traps and stationary currents captured by an active 1d model, *Physica A* **642**, 129763 (2024).
- [36] R. Klages and C. Dellago, Density-dependent diffusion in the periodic Lorentz gas, *J. Statist. Phys.* **101**, 145 (2000).
- [37] E. N. M. Cirillo, M. Colangeli, A. Di Francesco, M. Kröger, and L. Rondoni, Transport and nonequilibrium phase transitions in polygonal urn models, *Chaos* **32**, 093127 (2022).
- [38] E. N. M. Cirillo, M. Colangeli, M. Kröger, and L. Rondoni, Nonequilibrium phase transitions in feedback-controlled three-dimensional particle dynamics, *Phys. Rev. Res.* **5**, 043063 (2023).
- [39] P. M. Bleher, Statistical properties of two-dimensional periodic Lorentz gas with infinite horizon, *Journal of Statistical Physics* **66**, 315 (1992).
- [40] L. A. Bunimovich, On the ergodic properties of nowhere dispersing billiards, *Commun. Math. Phys.* **65**, 295–312 (1979).
- [41] L. A. Bunimovich, Y. G. Sinai, and N. I. Chernov, Statistical properties of two-dimensional hyperbolic billiards, *Russ. Math. Surv.* **46**, 47 (1991).
- [42] L. Bunimovich, C. Liverani, A. Pellegrinotti, and Y. Suhov, Ergodic systems of  $n$  balls in a billiard table, *Commun. Math. Phys.* **146**, 357 (1992).
- [43] N. Chernov, Statistical properties of the periodic Lorentz gas. multidimensional case, *J. Statist. Phys.* **74**, 11 (1994).
- [44] N. Chernov and H. K. Zhang, Improved estimates for correlations in billiards, *Commun. Math. Phys.* **277**, 305 (2008).
- [45] Y. Meir and N. S. Wingreen, Landauer formula for the current through an interacting electron region, *Physical review letters* **68**, 2512 (1992).
- [46] R. Murali, Y. Yang, K. Brenner, T. Beck, and J. D. Meindl, Breakdown current density of graphene nanoribbons, *Applied Physics Letters* **94** (2009).
- [47] M. Jönsson, R. Vedin, S. Gyger, J. A. Sutton, S. Steinhauer, V. Zwiller, M. Wallin, and J. Lidmar, Current crowding in nanoscale superconductors within the ginzburg-landau model, *Physical Review Applied* **17**, 064046 (2022).
- [48] T. Markovic, W. Huang, W. S. Huxter, P. Gambardella, and S. Stepanow, Intermediate diffusive-ballistic electron conduction around mesoscopic defects in graphene, *ACS nano* **19**, 12323 (2025).
- [49] E. N. M. Cirillo, M. Colangeli, A. Muntean, O. Richardson, and L. Rondoni, Deterministic reversible model of non-equilibrium phase transitions and stochastic counterpart, *J. Phys. A* **53**, 305001 (2020).
- [50] The presence of a horizontal channel does not alter the ergodic properties of the billiard dynamics. As proven in Ref. [40] (specifically, see Sec. 5 and Fig. 3b therein) the feedback-free version of our model belongs to the class of Bernoulli systems (called B-systems) and, consequently, possesses strong mixing

properties and ergodicity.

- [51] C. Cavoto, E. N. M. Cirillo, F. Cocina, J. Ferretti, and A. Polosa, Wimp detection and slow ion dynamics in carbon nanotube arrays, *Eurp. Phys. J. C* **76:349**, 1 (2016).
- [52] S. R. de Groot and P. Mazur, *Non-Equilibrium Thermodynamics* (Dover Publications, New York, United States, 1984) reprint of the 1962 edition published by North-Holland.
- [53] L. D. Landau, On the theory of phase transitions, *Zh. Eksp. Teor. Fiz.* **7**, 19 (1937).
- [54] M. Abramowitz and I. A. Stegun, *Handbook of Mathematical Functions with Formulas, Graphs, and Mathematical Tables* (Dover Publications, New York, United States, 1972).
- [55] M. Colangeli, A. D. Masi, and E. Presutti, Particle models with self sustained current, *Journal of Statistical Physics* **167**, 1081 (2017).
- [56] E. Toivonen, J. Kaipainen, M. Molkari, J. Keski-Rahkonen, R. Klages, and E. Raesaenen, Anomalous diffusion in the square soft lorentz gas, *Phys. Rev. E* **111**, 014216 (2025).
- [57] D. Szasz, Random walks and lorentz processes, *Entropy* **26**, 908 (2024).
- [58] P. Balint, H. Bruin, and D. Terhesiu, Periodic lorentz gas with small scatterers, *Prob. Theory Rel. Fields* **186**, 159 (2023).
- [59] S. Li, Rates of convergence for the superdiffusion in the boltzmann-grad limit of the periodic lorentz gas, *Stoch. Process. Appl.* **154**, 26 (2022).
- [60] M. Brown and P. Nandori, Statistical properties of type D dispersing billiards, *Discr. Cont. Dyn. Syst.* **42**, 4823 (2022).
- [61] F. Pene and D. Terhesiu, Sharp error term in local limit theorems and mixing for lorentz gases with infinite horizon, *Commun. Math. Phys.* **382**, 1625 (2021).
- [62] J. Vollmer, L. Rondoni, M. Tayyab, C. Giberti, and C. Mejia-Monasterio, Displacement autocorrelation functions for strong anomalous diffusion: A scaling form, universal behavior, and corrections to scaling, *Phys. Rev. Res.* **3**, 013067 (2021).
- [63] I. Fouxon and P. Ditlevsen, Refined central limit theorem and infinite density tail of the lorentz gas from levy walk, *J. Phys. A* **53**, 415004 (2020).
- [64] L. Zarfati, A. Peletskyi, E. Barkai, and S. Denisov, Infinite horizon billiards: Transport at the border between gauss and levy universality classes, *Phys. Rev. E* **100**, 042140 (2019).
- [65] L. Zarfati, A. Peletskyi, I. Fouxon, S. Denisov, and E. Barkai, Dispersion of particles in an infinite-horizon Lorentz gas, *Phys. Rev. E* **98**, 010101(R) (2018).
- [66] R. M. Feliczaki, E. Vicentini, and P. P. Gonzalez-Borrero, Dynamical transition on the periodic lorentz gas: Stochastic and deterministic approaches, *Phys. Rev. E* **96**, 052117 (2017).
- [67] D. Andreucci, E. N. M. Cirillo, M. Colangeli, and D. Gabrielli, Fick and Fokker-Planck diffusion law in inhomogeneous media, *J. Statist. Phys.* **174**, 469 (2019).
- [68] M. Kröger, Dataset: Fick's law and phase transitions in a feedback-controlled billiard system carrying a Lorentz channel, <https://github.com/mkmat/Lorentz-circuit> (2025).

### Appendix A: Numerical implementation of the LC

Quantities for the LC for comparison with the analytic predictions we obtain by following the deterministic trajectories of usually  $N = 1000$  point particles, initially placed with random velocity directions, fixed speed, and at random positions inside the circuit. Particles change their velocities during specular reflections at the Lorentz scatterers, at the var-

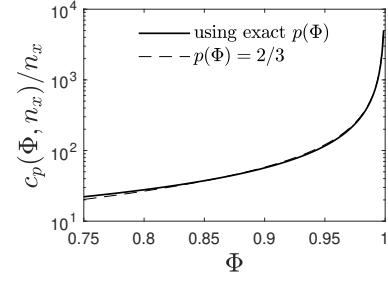


Figure 11. Mean number of collisions  $c_p$  divided by  $n_x$  of a single particle inside the passive channel, estimated using the trap crossing probability  $p(\Phi)$  (solid line) [25] and its approximate  $p(\Phi) \approx 2/3$  counterpart (dashed line) based on Eq. (A1).

ious circuit boundaries, or during feedback events. A feedback event occurs as soon as a set of particles residing within the active channel and sharing the feature  $xv_x > 0$  exceeds  $\Theta$ . During such event, the  $v_x$ -components of all particles belonging to the set are reversed. While the particle trajectories in the absence of feedback events can be calculated analytically from the collision points and collision surface normals, to test for the occurrence of feedback events, to measure the fluxes and mean urn occupation numbers, we keep track of the time-continuous trajectories that we construct from the collision times, locations, and reflected velocities. From Section III A one infers that the mean number of collisions  $c_p$  of a single particle inside the passive channel, taking into account both crossing and backscattering events, is

$$c_p(\Phi, n_x) = \frac{\tau_p}{\tau_{\text{trap}}} c_{\text{trap}} \approx \frac{\pi n_x \sqrt{\Phi} f(\Phi)}{1 - \sqrt{\Phi}}, \quad (\text{A1})$$

with  $f(\Phi)$  from Eq. (7). If  $N = 1000$  particles visit the passive channel just once, the total number of collisions is  $Nc_p \approx 10^7$  at  $n_x = 10$  and moderate area fraction  $\Phi = 0.9$ . Inline with Eq. (A1), this number increases dramatically upon approaching  $\Phi = 1$  (Fig. 11).

### Appendix B: How we deal with constraints

To test the transport law at constant energy difference  $\mathcal{F}\ell_p$  between the ends of the Lorentz channel we need to fix  $\bar{\chi} \in (0, 1]$  and  $\beta \equiv \xi/w_p$  and obtain (many) points on a straight line versus  $\ell_p$ . The LC has 8 independent model parameters mentioned in Section II. Assume we have identified a useful  $(\bar{\chi}, \beta)$  pair. To solve the problem we proceed as follows: (i) Choose 6 system parameters: positive  $n_x, n_y, \Theta, N \in \mathbb{N}$ ,  $w_a, w_p \ll r$  (they determine  $n, \ell_p$ ), (ii) Solve the following equation  $\ell_p/n_x = \ell_p/n_x$  for  $\Phi \in [\Phi_o, 1)$ :

$$\frac{\sqrt{3} w_p}{n_y} = \frac{\pi}{\beta w_p} \left( \frac{4}{p(\Phi)} - 3 \right) \frac{1}{1 - \sqrt{\Phi}}, \quad (\text{B1})$$

(iii) Calculate  $C$ , if  $C > 1$ , start over as there might be no  $\lambda$  for the choice of parameters. Note that  $C_{\text{max}} \approx 0.04 w_p/w_a$ , (iv) Find one or two solutions  $\lambda(\Theta, C)$  from Eq. (24) (taking

into account stability issues), ideally at least one exists. If not, start over, (v) Calculate  $\ell_a = 8\lambda(\Theta, C)A_u(n_y, n, w_a)/Nw_a$ .

This was the last LC parameter to be specified, (vi) Proceed until a dense set of  $\ell_p$  values has been created.